The Nigerian Institute of Mechanical Engineers
34th International Conference and Annual General Meeting (2021)

INVESTIGATION OF PRELIMINARY FACTOR LEADING TO FIRST-THIRD STAGE BLADE CRACKS INITIATION, GROWTH AND THEIR EFFECTS ON AERO-ENGINE PERFORMANCE

I.O. Otaiku[1], I. K. Adegun[2]

[1]International Aviation College, Ilorin, Kwara State
[2]Department of Mechanical Engineering, University of Ilorin, Kwara State, Nigeria
Corresponding Author olaoluwaotaiku@yahoo.com. +23460520474.

Abstract

The paper presents the preliminary temperature leading to first-third stage blade cracks initiation, growth and their effects on aero-engine performance. The temperatures were determined by Scan Electron Macroscopy installed with optical camera while mechanical loadings at specified temperatures were obtained by means of tensile testing machine. Ti-6Al-4V, AISI 403 cadmium stainless steel and INC 718 were the three blade materials investigated. 1st stage axial and single stage centrifugal compressors; 2nd& 3rd stage axial compressor; and single stage axial gas turbine blades were respectively considered for Ti-6Al-4V, AISI 403 stainless steel and INC 718. The ranges of temperature considered for Ti-6Al-4V, AISI 403 stainless steel and INC 718 were 450 – 550K , 250-500K and 1083-1235K respectively. Chemical compositions and microstructures of the materials were investigated. The observable heat treatment time for all the materials were from 1-8 h. 20 - 70 kN forces were applied on the three materials and their elongations were plotted against the corresponding forces. Results showed that their chemical compositions at room temperature were the same even after several heat treatments while their microstructures were at variance. Stability in the microstructures without cracks was attained at temperature range of 500 to 520K for 1h for Ti-6Al-4V, 450 -480K for 30-45 min for AISI 403 stainless steel and 1083 -1200K for 2 h for INC 718. Beyond these temperatures, crack initiations and growths were noticed for Ti-6Al-4V, AISI 403 and Ni-alloys. In the three blades' alloy, γ', $\gamma''$and δ grain elements for each material showed that their γ',γ'' were thermodynamically stable at room temperature. However, the cause of crack growths was due to changes in grains sizes and the rafting of the precipitates in the blade specimens. The results also indicated that for 2 mm cracks size on stainless steel alloys, the maximum allowable number of cycles for failure to occur is $10^6$and for a crack size of 3 mm on Ti-6Al-4V alloy and 6.5 mm on Ni alloy blades, the maximum allowable number of cycles to failure is 10^8; beyond these allowable cycles, fracture or rupture becomes inevitable.

1. INTRODUCTION

The failure mechanisms of Ti6Al4V titanium alloy , AISI 403 stainless steel of compressor blades and INC 718 nickel alloy of turbine blades in the low and high pressure and temperature sections of an aero-engine PT6T BE/BG have emerged due to deterioration or degradation of metallurgical and mechanical properties of the blades. Fatigue due to crack initiation sites, crack growths and margin leading to failure or fracture at different temperature and stress loadings have been investigated to be the cause of poor engine performance, increase in downtimes and maintenance costs. Hence health monitoring techniques to forestall these anomalies has to be well articulated to solve the prevailing problems in the aviation industry in local depots.

The choice of materials depends on the section of the aero-engines, especially in gas turbine. Materials frequently used in the first stage rotor and stator blades of the compressor sections are Titanium-based superalloys (AFM – Pratt & Whitney, 2014). The second and other stages are made up of AISI 403 cadmium-stainless steel alloyed element (Khalid et al., 2021; Chizhi et al., 2021; Moradi et al., 2021; Srinivas et al., 2019; AFM P & W, 2014 and Luque , 2017). This study will look in details at the behavior of these three materials, at different operating temperatures for compressor-turbine section of PT6T BE/BG turboshaft engine. The three different blade specimen materials being investigated included: 1st to 3rd stage axial compressor (1st stage – Ti-6Al-4V and AISI cadmium-stainless steel for 2nd and 3rd), another 1st stage centrifugal compressor (AISI 403 stainless steel alloy) and finally, 1st stage of axial gas generator turbine of the PT6T-BE/BG Pratt and Whitney turboshaft engine). Engine specifications have weight of 299 kg, overall dimension length of 1670.05 mm by 1104.14 width by thickness of 8.26 mm. Thermal efficiency is 22% and power output is 1193 kW. Other important parameters are as shown in Table 1.0. Figures 1a and b showed the specimen blades and sections being studied.

In several aero-engine fault detection, component degradation and their originated causes in gas turbine engines studies, deterioration of matrix element and other coherent strengthening agents in first blade section only have been widely published (Steere et al., 2017); Rajedran, 2018; DiMarco, 2020; Bela, 2018; Amir &Shervin, 2018; Alqallaf et al., 2020; and Kai et al., 2020). Little or no attention has been paid to stages above the first stage because of cost implications and time constraints involved, hence this research will probe further into other stages to determine the temperature leading to initial blade cracks and their growths in compressor-turbine sections of the engine. In this paper, investigation of the initial temperature leading to first to third stage blade cracks and the effect of crack growths on aero-engine performance will be studied. This process will determine the chemical composition and examine the microstructure of un-cracked blades of three stages of axial compressor, single stage of centrifugal compressor and axial turbine of a PT6T-3BE/BG engine; determine the temperature leading to initial crack for each stage and examine crack growth and theirmicrostructures after crack for different temperature ranges.

2. MATERIALS AND METHODS

2.1 Preparation of Samples

Ten ex-service rotor and four stator blades of 1st to 3rd axial compressor stages, single stage rotor/stator for both centrifugal compressor and axial turbine without cracks were first extracted from one of the unserviceable PT6T 3BE/BG engines from the Nigerian Police Air Wing Helicopter based in Abuja. After extraction, they were selected and further subjected to visual and microscopic examinations without heating using SEM. A total of 30 rotor blades, 12 stators were examined, but only the rotors were prepared for further examinations and investigations.The identified un-cracked rotor blades were cut into size of 50 mm length and 30 mm width using small handheld electrically powered

cutting wheelsto enable proper mounting on the laboratory equipment at room temperature in accordance to ASTM E8. Thereafter, the blades were well cleaned, polished and etched.

2.1.2 Polishing

The un-cracked blades with aforementioned sizes were fine polished to 1pm to reveal the microstructure for various temperatures following Zhou et al. (2016) and Doux and Vincent,(2019) procedures using the Polishing machine (UltraPol) shown in Figure 1.

2.1.3 Etching

The three blade set were etched using a solution of 50 ml HCl, and 15ml $HNO_3$with addition of 100 cl of water each in order to determine a better etchant between the two acids. The acid that produced better contrast between γmatrix, γ', γ'' precipitates and δ grain boundary agentin the etched specimens were immersed for 150 mins to remove oil, grease and other micro-particles that might impair homogenous heat treatment process as shown in Figure 2 a), b) and c). The bladespecimens were left to dry after immersion (Blachino, 2014; Blachinoet al., 2014 and 2015 and Excobar –Moreno et al., 2019) as shown in Figures 2 and 3.Figures 3 a), b) and c) showed ex-service Ti-alloy, Ni-alloy and AISI 403 blades before polishing, etching and heat treatment.



Figure 1: Polishing Machine.
Location**:** KWASU, 2020



Figure 2a: Immersion of specimens in HCL etchant



Figure 2b: Change in colour after immersion



Figure 3a:1ststage blade axial compressor

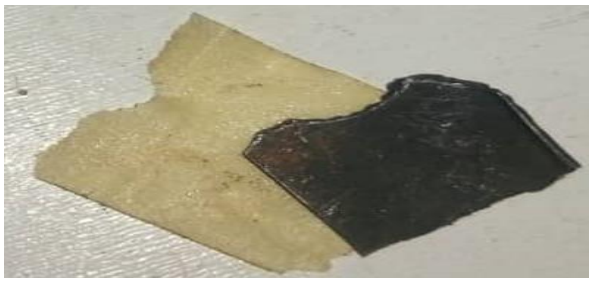


Figure3b:1st axial gas generator turbine blade



Figure 3c: 2nd and 3rd Stage Axial Compressor blade.

The etched and un-cracked specimens were as shown in Figures 4 a, b and c.



Figure 4a: un-cracked and etched specimen



Figure 4b: 1st stage blade axial compressor (LHS) and axial gas generator turbine blade (RHS) after polishing, and etching.

2.2 Chemical Analysis of the Specimen Blades

The chemical composition and analysis of each un-cracked blade materials per stage were carried out using SEM and constituent matrix and precipitate elements for the blades were obtained and recorded.

2.3 Microstructural Examinations and Analysis of Un-cracked Blade Materials

A 50 mm length by 30 mm width un-cracked rotor blades were mounted on the SEM at room temperature without pre-heating or mechanical loading to determine their microstructures, which was to serve as control for other microstructures during different stages of heat treatment and loading conditions. In the SEM (installed with thermographic Leica EC3 camera and processed by the LAZ EZ 2.0 software), a 15kV and 10mm working distance was observed.

2.4 Examinations of Grains Sizes and Areas of γ Matrix and other Hardening Agents

The microstructural grains sizes, areas for γ elements,γ', γ'' precipitates and δ grain boundary agents for 1st to 3rd stage axial compressor, single stage centrifugal and axial turbine bladeswere determined and characterized using the light optical microscope and Microsoft Image Composite Editor installed with SEM.

2.5 Heat Treatment Procedures

2.5.1 Temperature leading to crack initiation

The furnace with an automatic regulation and a heating system of 80 kW was used for the heat treatment stages.The working chamber has a 500mm x 400mm x 400mm working area, and is equipped with a set of nine sleeve-protected thermocouples with a temperature measurement accuracy of ±3°C as shown in Figure 5.The specimen microstructure was studied for each temperature raised while applying tensile load 20-70 kN between 10^{-4} to 10^{-1}strain rate (at a quasi-static strain rate of approximately 0.001 $s-1$). There were about 10 scans obtained for each blade specimen from theunloaded state to final fracture. In the furnace, three characteristics were recorded: ramp up rate, the dwell time (aging) and the cooling rate for each blade per stage. These were to determine the crack initiation spots on the un-cracked blades, growth and margin for total fracture during heat treatment processes.

The exact temperature distribution of the furnace wall was determined by varying the control temperature from 400 – 550 K forTi- alloy, 250 to 500 K for stainless steel and 1083 -1250 K for Ni alloy in a step of 50 K per 60mins each as shown in Figure 5 and using SEM (Hitachi S-3400) being similar to the equipment and procedures employed by Farokhi (2014), Okura (2015) and Blachino et al. (2016).

The temperature and tensile stress/strain leading to crack initiation, growth and the margin before permanent failure or rupture were obtained and their microstructures were captured by SEM and servo-hydraulically operated tensile machine as shown in Figures 6 & 7.

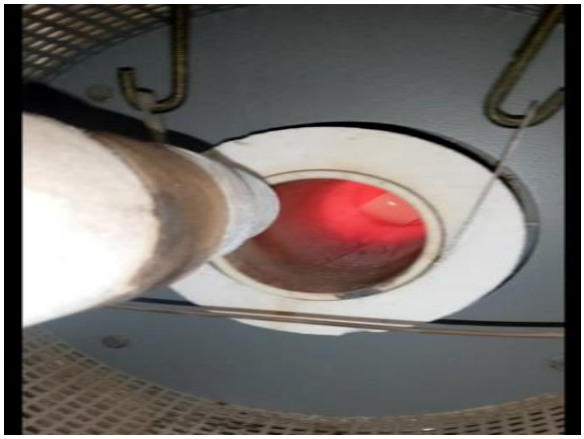


Figure 5a: Furnace Inner Chamber



Figure 5b: Indicator Panel

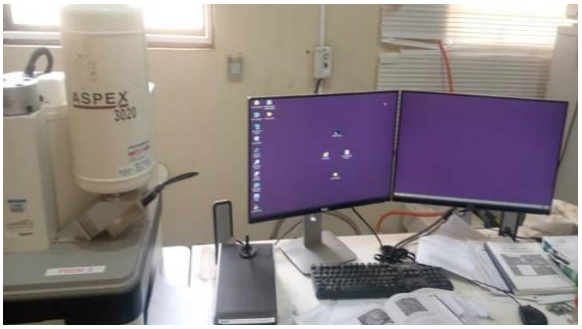


Figure 6: Scan Electron Macroscopy Machine (SEM)



Figure 7: Servo Hydraulically operated Tensile Machine (Instron 300LX-J3 Universal Mechanical test)

2.6 Degradation of Microstructure after Heat Treatment

2.6.1 Determination of crack growth

Tensile force was varied between 20 - 70kN (Bingert, 2013; Nemcko et al., 2016;

andSrivastava and Needleman, 2016) and applied for a number of cycles (hour) using vibration machine for blades with initial cracks from tensile loadings. Since the shaft rotation of the turbine generator is 38,100 RPM, at this speed, stress accumulation should aggravate on the cracked blades, then material yield strength would reduce and permanent deformation inevitable. Therefore to determine these states, the frequency of the vibration machine was carefully increased from 50 to 100Hz (NASA, 2015; Garret, 2017 and Chizhi et al., 2021). This is to compensate for high cycle fatigue HCF that they might experience in real life operations. The crack growths during the application of tensile force and HCF values were recorded.

2.7 Fracture Testing

After the determination of crack initiation and crack growth, each sample of the material is mounted on a vibrator machine and fatigue is simulated on each material between 5 g to 25 g range. The number of cycle, amplitude of acceleration (different intensity of vibration, which was defined by amplitude of acceleration of the movable vibrator head) and crack length for permanent fracture was then recorded. Crack lengths until fracture was determined by measuring crack opening displacement with a clip gauge extensometer at 12.0 kN and 1.2 kN (R= 0.1) and 20 Hz.

3. Experimental Results& Discussions

3.1 Chemical Composition

The chemical composition analysis showed the result of the un-cracked blades of 50 mm length and 30 mm width of Ti, AISI 403 and Ni alloys after service life of 10,000 h each. Their compositions (constituent elements) at room temperature was the same even after several heat treatment carried out according to this work, and was very close to previous results from other scholars and the manufacturer's specification (Meher-Homji et al., 2009; Bousser, et al.,

2014;Jovanović et al., 2016; Bai et al., 2020; and Bahramnia, et al., 2020).

The compositions for all the blades per stage per section were as shown in Tables 1 and 2.

Table 1: Chemical Composition of the Compressor –Turbine Blade before Heat Treatment

Sample Wt %	Validation		Current Result		Validation		Current Result			Validation	
	1st Stage Axial& Single Stage Centrifugal Compressors		1st Stage	2nd Stage	2nd and 3rd Stage		3rd Stage	Single Stage Comp	Single Stage Axial gas Turb	Singe Stage Axial Gas Gen. Turbine	
	(Meher-Homji et al., 2009	Bousser et al., 2014)	Ti-6Al-4V	AISI 403	Bai et al., 2020	Bahramnia et al., 2020	AISI 403	.Ti-6Al-4V	INC 718	Meher-Homji et al. 2009	Bousser et al., 2014
AL	6	6	6	------	---------	--------	----------	6	0.8	0.6	0.6
Ti	78	79	80	----------	----------	---------	----------	80	0.8	0.8	0.8
Cr	---------	----------	----------	12.2	13.0	12.2	12.2	--------	19.5	19	18
Ni	--------	----------	----------	-------	-------	--------	--------	----------	56	54	55
C	0.20	0.25	0.25	0.15	0.1	0.15	0.15	0.25	0.02	0.05	0.05
Fe	---------	--------	--------	80	84	82	80	-------	19.5	19	18.5
Mo	0.5	0.5	0.5	---------	--------	---------	----------	0.5	3.0	3.0	4.0
B	---------	----------	----------	0.05	0.05	0.05	----------		0.0004	0.0004	0.0004
V	4	4	4	---------	--------	---------	----------	4		-------	-------
Cb				---------	--------	---------	----------		5.4	5.2	5.5
Cd	----------	----------	----------	6	----------	6	6	---------		----------	-------
Nb	0.4	0.4	0.4	0.015	0.015	0.015	0.015	0.4		---------	--------

Table 2: Material Element Symbols

Element	Aluminium	Titanium	Chtomium	Nickel	Carbon	Iron	Mplybdenum	Boron	Vanadium	Cobalt	Cadmium	Niobium
Symbol	Al	Ti	Cr	Ni	C	Fe	Mo	B	V	Co	Cd	Nb

3.2 Microstructural Examinations and Analysis of Un-Cracked Blade Materials

The result of the microstructures, examination of morphological sizes and characteristics of the γ matrix, γ' and γ''precipitates and δ grain boundary agents before heat treatment in all the three materials investigated were as shown in Table 3 and Figures 8 to 12.

Table 3: Matrix Element γ, precipitates γ' / γ'' and the grain boundary precipitate δ for each blade per stage/section

Stage	Materials	γ	γ'	γ''	δ
1st (axial)	**Ti-6Al-4V**	**Ti**	**Ti_3Al**	**Ti_3Nb**	**Ti_3Nb**
2nd (axial)	**AISI 403**	**Fe**	**$M_{23}C_6$**	**------**	**M_6C_8**
3rd (axial)	**AISI 403**	**Fe**	**$M_{23}C_6$**	**------**	**M_6C_8**
1st Centrifugal	**Ti-6Al-4V**	**Ti**	**Ti_3Al**	**Ti_3Nb**	**Ti_3Nb**
1st Turbine	**INC 718**	**Ni**	**Ni_3Al**	**Ni_3Nb**	**Ni_3Nb**

M_{23} could represent titanium, nickel, tantalum, boron and magnesium (Antunes et al., 2016).

Figure 8 showed the microstructure of the 1st stage dendritic structure of Ti – alloy before heat treatment (Ti- 6AL- 4V) that the γ^i, γ'' microstructure in the dendritic region (black spot) with theirspherical-shaped γ'' precipitates were regular and evenly distributed in the γ matrix of the main element while γ′ andγ'' -$M_{23}C_6$ carbides without δ -phases were not observed in samples of 2nd and 3rd stages of axial compressors which were made up of AISI 403 stainless steel alloy as shown in Table 3.

Like Yao et al. (2012); Zhou et al. (2013) and Ramsperger et al. (2016) results, it was discovered, as shown in Table 1 for chemical composition, the percentages of Al, Ti and Ni were not found in 2nd, 3rd axial compressor therefore the formation of γ'' and δ-phase were negligible or not even available because they (AISI 403) operate in lower temperature than 1st stage blades (Segersäll et al., 2015 and Wang et al., 2016).

Microstructure of Fe – alloy (AISI 403) for 2nd and 3rd axial compressor before heat treatment showed regularity in intermetallic element of the blades as shown in Figure 9

and similar to the 1st stage blade (Ti-alloy) already explained.Figure 10 showed the microstructure of the INC 718 before heat treatment.

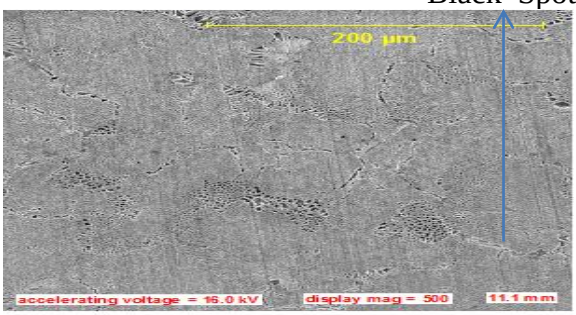


Figure 8: Microstructure ofTi- 6AL- 4V for 1st stage axial andsingle stage centrifugal compressors.

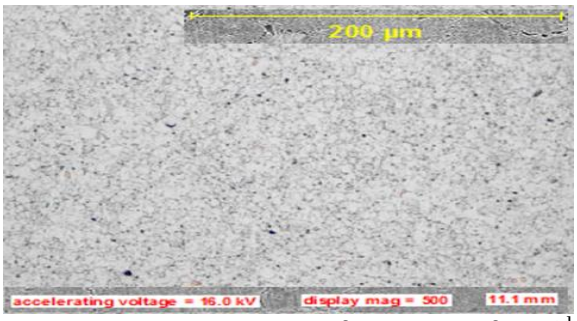


Figure 9:Microstructure of AISI 403 for 2nd, 3rd axial compressor before heat treatment

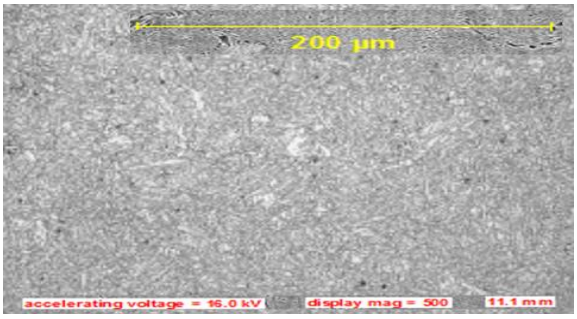


Figure 10: Microstructure of INC 718 before heat treatment.

Under Light Optical Microscopy LOM, γ matrix was observed for Ni based superalloy made up of 56% (faced Cubic Centre) as shown in Table 1. Theγ', γ'' were Ni_3Aland Ni_3Nb and $\delta$was Ni_3Nb. The microstructures in the matrix were the black spherical-shaped precipitates coherent in the matrix while δ was found at the grain boundaries when examined at room temperature (Maktouf and Saï, 2015 and Russell, 2015). From the observation, it was concluded thatγ', γ''were thermodynamically stable at room temperature. This was used as a control for further heat treatment. It should be noted that from the results obtained at room temperature for the three blade materials, microstructure close to the leading edge of each blade was the same as the microstructure close to the trailing edge and the chemical composition is the same for each blade materials at various temperature studied.

3.3 Temperatures Leading to Crack Initiation in the Blade

The heat treatment methods to obtain initial cracks the minimum suitable time without cracks was approximately 30 -60 mins with no prior deformation under applied load and stress above the room temperature. A load between 20-70 kN were applied for all the materials and heat treatment aging times from 1-8 h were maintained. The results showed that for Ti-6Al-4V there was stability at 500 to 520 K for 1h, for AISI cadmium- stainless steel, its microstructure was seen to be maintained at 450 K for 30-45 mins without cracks at the same applied load. And INC 718 was stable for 2 h when operated at 1083 K under the same applied load. But crack presence was noticeable for Ti, AISI 403 and Ni-alloys at their various temperatures after the aforementioned temperatures and hours were exceeded at the constant load as shown in Table 4.

The values of grain sizes obtained using the technique of Escobar-Moreno et al. (2019) were comparedwith the values of δ phase , γ matrix, γ' and γ''precipitates obtained upon cooling to room temperature. Since the aging time for specimens from compressors and turbine were only 5 -8 h the results obtained as validated by Wang et al. (2017), in long aging times during the service temperature, γ″ decompose into stable δ (Ni_3Nb) phase. There was a close correlation between δ and γ″ precipitates because they contained same evolution of Nb content in the matrixes of Ti and Ni-alloys being investigated(Khan and Bashin, 2017).

Table 4: Heat Treatment per Stage

Temperature °C	Ramp up rate mins	Dwell hrs	Aging hrs	Materials	Elongation %
150 to 300	10	1/3 to ½	5	Ti-6Al-4V	10
100 to 200	10	½ to 1	5	AIS	7.8

				I 403 – Cd	
800 to 950	**10**	**2**	**5**	**IN 718**	**5**

It was observed that the crack propagated at a relatively steady growth rate since it was done in an automatic regulated furnace and could be assumed that a constant crack growth rate occurred during the heat treatment processes as shown in Table 5.

Table 5: Heat Treatment Stages with Material Elongation (%)

Parameters	Materials		
Ramp up rate	Ti – alloy	AISI 403 – Cd	INC 718
Dwell h	2	2	2
Cooling h	5	5	5
Temperature K	400 to 550	150 to 500	800 to 950
Strain rate/s	0.0005	0.0005	0.0005
Elongation %	0 to 10	0 to 7.8	0 to 5

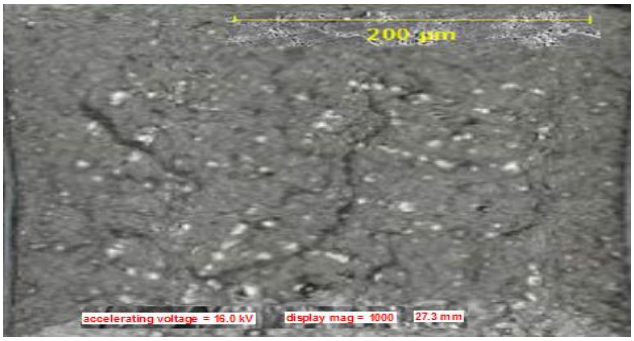
3.4 Axial and Centrifugal Compressors and axial Gas Generator Turbine Stages with Crack Initiations

The results obtained as shown in Figure 11 a) and b) for 1st stage axia**l** and centrifugal compressors blade material showed that significant changes in the microstructure of the Ti - base alloy during heat treatment occurred between 400 to 550 K and validated by similar values specified in the aircraft manual, Clark (2000); Zhou et al. (2018) and Kyaw et al. (2017). Figure 12 a) and b) showed crack initiation at the γ matrix and γ' of the precipitates of 2nd and 3rdaxial compressor blade material - AISI 403 cadmium stainless steel. The γ'precipitatesat high temperature (400 to 500 K) were seen to be disorderly arranged during heat treatment thereby leading to dislocations and cracks which was different from its orderly arrangement at room temperature.

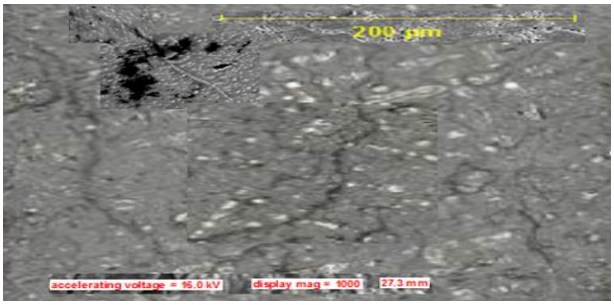
The primary γ'' particles of single stage axial gas generator turbine was observed to

be spheroidal while the precipitates were coarsened as shown in Figures 13 a) – c) during heat treatment which was similar to the results of Kyaw et al., 2017 and Li et al., 2017 for similar material. The results showed the crack initiation was between1083 -1193 K within 2 ½ h heat treatment. From the observations when held at above 1100K temperature, a visible crack could be seen and felt by touch at the coarseand the fine grain regions whereas in 1083 K for 1hr, the even grain size distribution maintained. At temperature above 1100 K, applying 175 MPa stress level, the microstructure of single crystal nickel-base alloys became unstable with respect to the changes in morphology of γ' precipitates. Rafting of γ' articles occurred under service conditions in turbine blades as well as under laboratory conditions (either the blades were static or rotating) according to Escobar-Moreno et al. (2019).

Ti-alloy Blade Microstructures



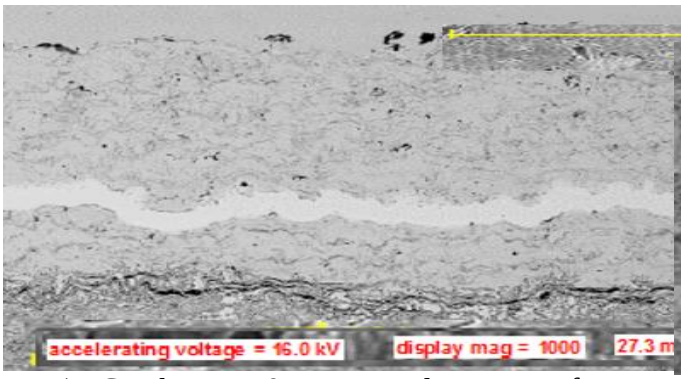
a) Crack initiation at 520K at tensile stress of 175MPa for 3 ½ h



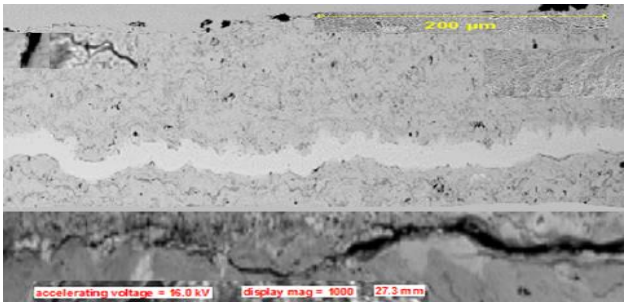
b) Crack at 530K at tensile stress of 175 MPa for 3 ½ h

Figure 11 a) and b): Crack initiation at the γ matrix and γ' of the precipitates of 1st stage axial and centrifugal compressors blades (Ti-6Al-4V)- a) at 520K b) at 530K

AISI 403 Cadmium Stainless Steel **INC 718**

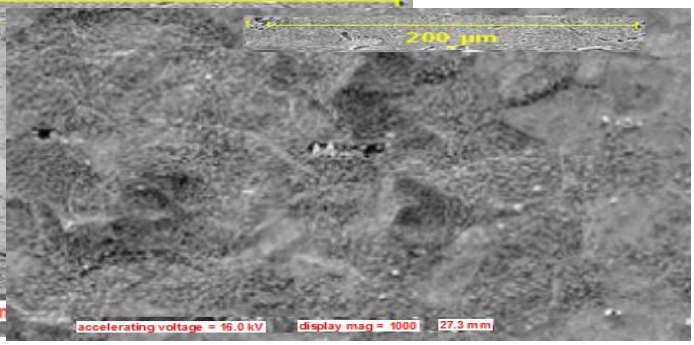


a) Crack at 450K at tensile stress of 175MPa for 3 ½ h

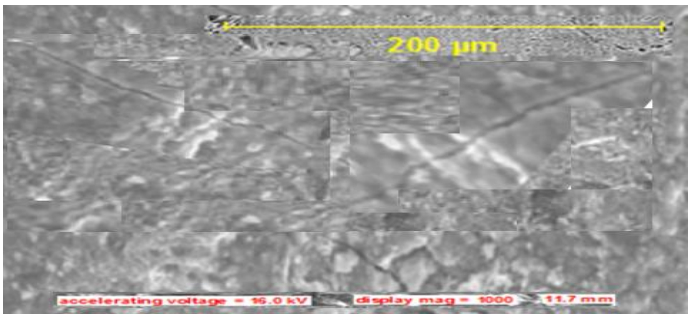


b) Crack at 500K at tensile stress of 175MPa for 3 ½ h

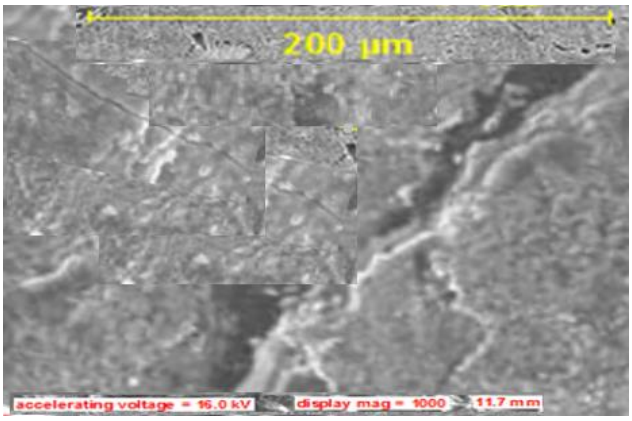
Figure 12:Crack initiation on AISI 403 cadmium stainless steel. a) and b) Cracks at 450K and 500K at tensile stress of 175MPa for 3 ½ h.



a) Coarsening of grains 1100K at tensile stress of 175MPa for 2 ½ h



b)Coarsening of grains and cracks initiation at 1183K at tensile stress of 175MPa for 2 ½h



c) Cracks at 1200K at tensile stress of 175MPa for 2 ½ h

Figure 13 (a - c): Crack initiation on Inconel 718 between1083 to 1200 K.

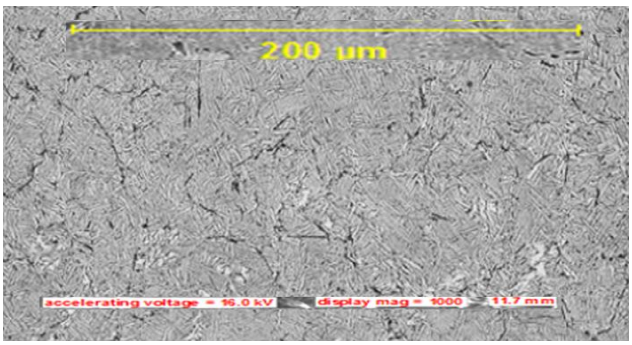
3.5. Crack Propagation and Rate of Crack Growth

Propagation of the different cracks occurred by steady crack growth because of the regulated temperature and ageing, especially more at a low density area than higher density area with stress level intensity on the blade being considered. This was noticed for all the blades

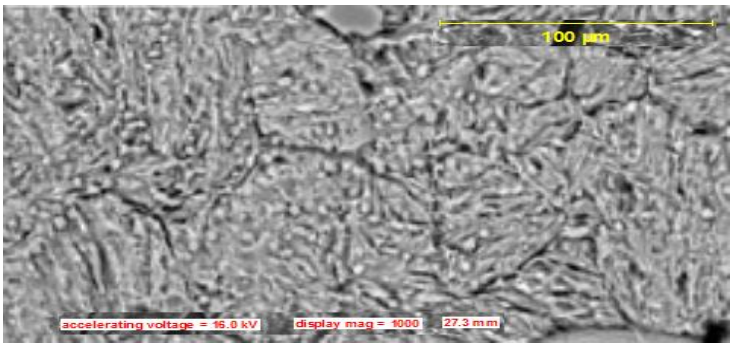
A characteristic temperature of 520 K or above for 1 h could be identified as the temperature for γ' dislocation or crack initiation which corresponded to the γ' temperature range for the Ti-alloy from the manufacturer and many literatures (Kumar and Kandasubramanian, 2016). For Ti alloy, γ' and γ''were responsible for different behavior distributions of the alloying elements and their homogeneity. During heating, the as-received material, the smallerγ' precipitates in the dendrite core were the first to dissolve due to their high surface energy. At higher temperatures, the much larger γ''precipitates within the interdendritic regions start to dissolve as shown in Figure14 a) to c).

From the observations, in Ti-6Al-4V alloy samples, the length scale on which segregation occurred was very small compared to AISI 403 steels. Thus, the interdendritic area was very small and similar to the sizeof the γ, γ' precipitates.The γ' particles could not be found in the γ matrix of the AISI cadmium stainless steel because of high temperature effect that might have caused the incipient melting of coherent precipitate as shown in Figure 15 a) and b). The microstructure corresponding to the compressor blades showed that γ' particles in stainless steel material, although rather small, were still present in the γ matrix of the main element even beyond the operating range as specified in the AMM but reductions in volume

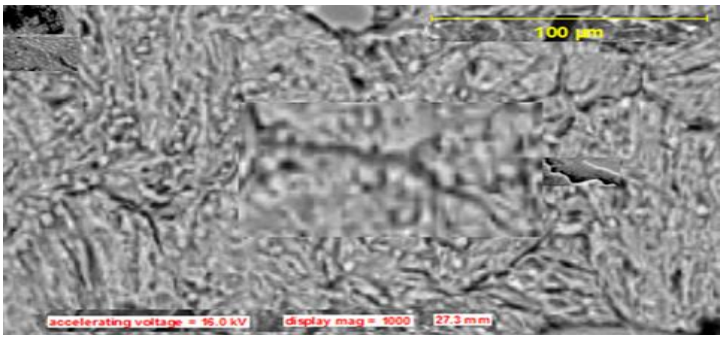
fraction as a result of elevated temperature was significant (Hanus and Ruzicka, 2018) . This reduction in the fraction of volume of the $M_{23}C_6$ carbide was primarily the cause of crack growth as observed during aging. In this blade stages, presence of iron (Fe) as the main element, allowed the compound of carbides which could be of titanium, tantalum, iron, magnesium and chromium and nickel (Clark, 2000 and Antunes et al., 2018) to play a major role in the crack propagation as shown. Figure 15 showed the propagation of the AISI blades at temperatures near 500 K and above. In Figure 16 a) - d), the crack growth in γ', γ'' and margin to fracture or permanent failure during elevated temperatures for INC 718 was as shown. Crack at the tips occurred at temperatures at 1200K, the grainboundaries around the edge of the crack increased much faster along such boundaries thereby increasing the crack sizes.



a) Growth in Ti –alloy at 520K at tensile stress 150MPa for 5 ½ hrs



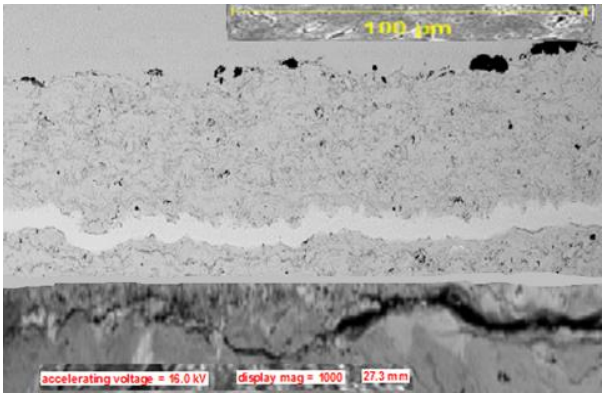
b) Growth in Ti –alloy at 530K at tensile stress 150MPa for 5½ h



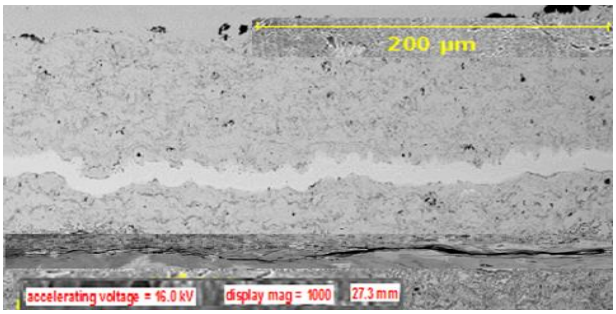
c) Growth in cracks in Ti –alloy at >550K at tensile stress 150MPa for 5 ½ h.

Figure 14 (a-c): Growth in Ti –alloy between 520K and > 550 K for 5 ½ h at 150 MPa.

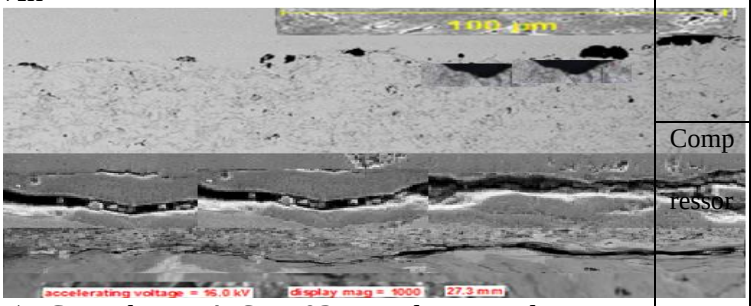
AISI 403 Cadmium Stainless Steel



a) Growth in AISI 403 stainless steel at 450K at tensile stress 150MPa for 5 ½ h



b) Growth in cracks in AISI 403 stainless steel at 480K at tensile stress 150 MPa for 5 ½h



c) Growth in AISI 403 stainless steel at 500K at tensile stress 150 MPa for 5 ½ hrs

Figure 15: Growth in AISI 403 at 450 - 500K. a) 450K b) 480K c) 500K for 5 ½ dwell (aging) time at 175 MPa.

Crack growth was evident in the microstructure at above the normal operating temperature especially during the dwell time at above the specified temperature as given in Table.6. The normal operating temperature of the compressors and turbine sections were shown in Table 1.0 and grain sizes, areas for the materials during heat treatment were as shown in Table 6.

Table 6: Temperature range between crack growth and margin to fracture with grains sizes.

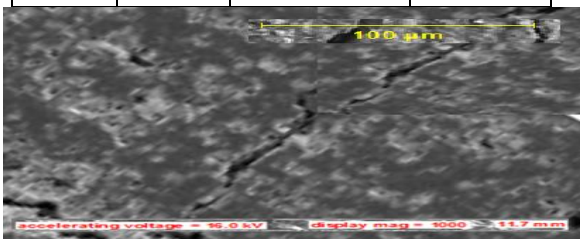
Section	Materials	Stages	Temp.K	$\gamma\mu$ m^2	Grain diameter μm	γ''	δ μm^2
Compressor	Ti-alloy	1st& 1st Cent	400	0.33	0.007	0.075	
			520	0.36	0.006	0.045	
	AISI Steel	2nd& 3rd (Axial)	350 500	0.39	0.007		
Turbi	INC	1st	700	183.	11.02	124.	243

ne	718	Stage (axial)		73		4	
			800	177.14	10	121.7	290
			900	176.25	9.5	119.3	152

The elongation results of the three blade materials were shown in Table 7 for their

Table 7: Elongation during Heat Treatment

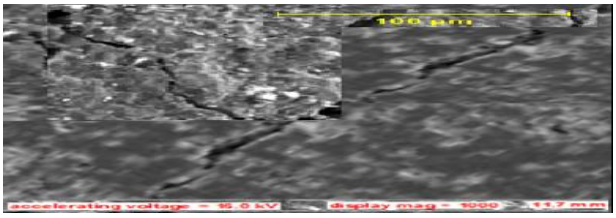
Materials Temp K	Elongation % 400-550	Elongation % 250 to 500	Elongation % 1083-1250
Ti-alloy	10 – 26	5 – 22	-
AISI steel	-	2 to 7.8	-
Nickel	-	-	2.5 – 36



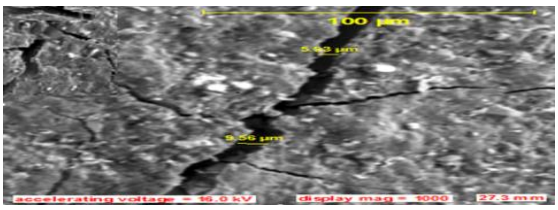
a) Cracks at 1200K at tensile stress of 150 MPa for

respective temperature ranges. The stainless steel tempered at 490K revealed that gamma prime $M_{23}C_6$precipitates with an average length of 195 nm (Hanus and Ruzicka, 2018). Precipitates with an average diameter of 8and 10 nm were also observed for the titanium and nickel materials respectively.

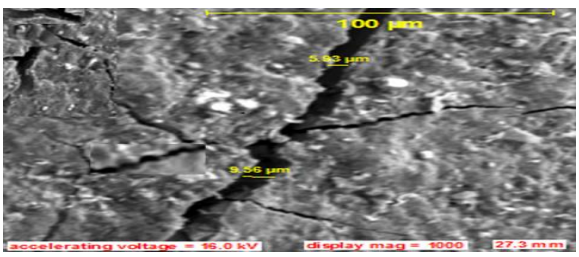
4½h



b) Cracks at 1210K at tensile stress of 150 MPa for 4 ½ h



c) Cracks at 1220K and 1230K at tensile stress of 150 MPa for 4 ½ h



d) Cracks at 1235K at tensile stress of 150MPa for 4½ h

Figure 16 (a-d): Crack Growth Microstructure of INC 718 Ni-alloy at Gas Generator Turbine

3.6 Crack Growth Microstructure at High Stress

For the high cycle fatigue analysis of the blades microstructure, the crack growth was faster and time to rupture or permanent failure was quicker than when the stress applied was lower as already explained in Figures 6 to 8 for all the materials.

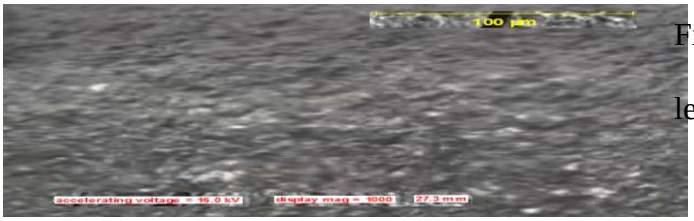
However, at 1235K for Ni-alloy, 570K for Ti-alloy and 500K for Stainless Steel materials and at stress load of 960, 700 and 600 MPa respectively, between 30 mins to 1h, γ'precipitates showed cuboidal morphology for all the aging times and the distribution changed from a bimodal to a unimodaldistribution for all the materials. But at temperature above 1235K aging time beyond 1h, the unimodal distribution and morphology of the precipitates for Ni alloy bladechanged from spherical to irregular morphology as shown in Figures 6b and 8b similar to the microstructure when a low stress was applied. For the increasing isothermal temperatures, the hardness measurements for each temperature from the previous section, has shown that the values don't change much for the increasing heat treatment times, even though there are changes in the γ' size, morphology, and distribution type for the isothermal temperatures and times (Kyaw et al., 2017 and Liu et al., 2017).

3.7 Microstructure at Fracture Stage

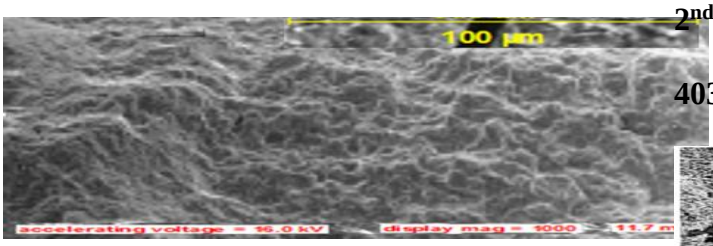
Low and High cycle fatiguewere usually caused by vibration, surge or a large change ofcentrifugal load during startups and shutdowns, fractured blade microstructures were as shown in Figure17 when subjected to 175 MPa for a certain period at increased temperatures to determine when the fracture occurred. As shown in Figure 4.17a) to c) for Ti alloy, 4.18 a) and b) for Stainless

Steel alloy and 4.19 a) to d) for Ni alloy. The failure was observed to have occurred at the area that maximum stress was most concentrated for all the materials.

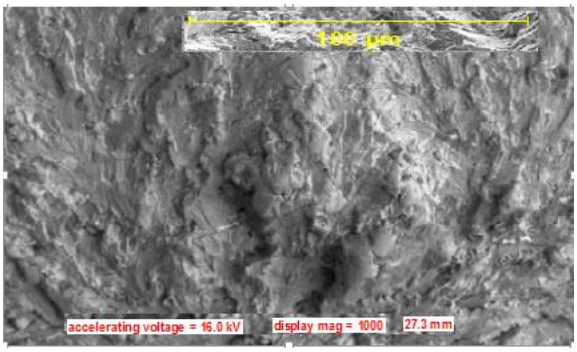
Ti-alloy- 1st Stage Axial and Single Stage Centrifugal Compressors



a) Fracture of the Ti – alloy blade at 550 K at 150MPa 4 ½ h



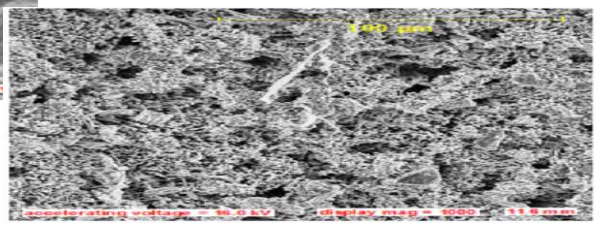
b) Fracture of the Ti – alloy blade at 560K at 150 MPa for 4 ½ h



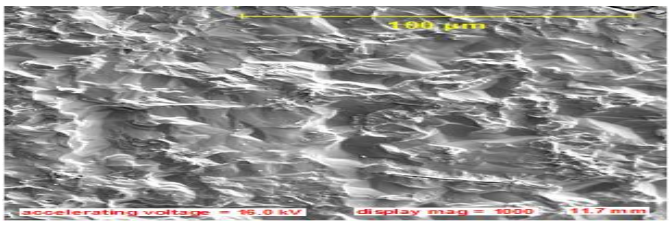
c) Fracture of the Ti – alloy blade at 570K at 150 MPa 4 ½ h

Figure 4.17 a) to c): Stages of crack growths leading to fracture in Ti alloys

2nd and 3rdStages AxialCompressor -AISI 403 Cadmium Stainless Steel



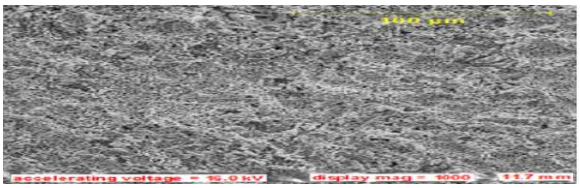
a) Fracture of the AISI stainless steel alloy blade at 520K at 150MPa 2 ½ hrs



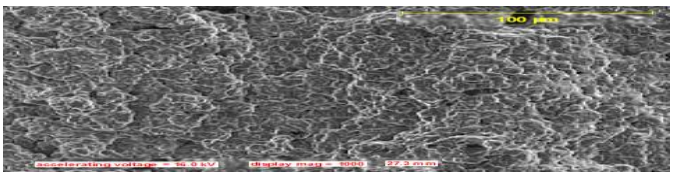
b) Fracture of the AISI stainless steel alloy blade at 520K at 150 MPa 2 ½ h

Figure 4.18 (a-d): Microstructure of Ruptured Ti-6AL-4V 1st stage blade at 500K and tensile stress of 175 MPa.

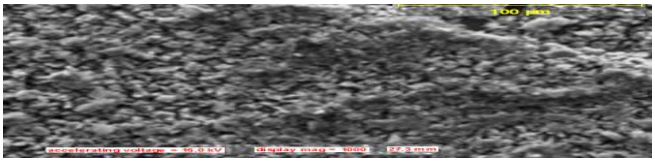
Single Stage Axial Gas Generator Turbine INC 718 Blade 1250K



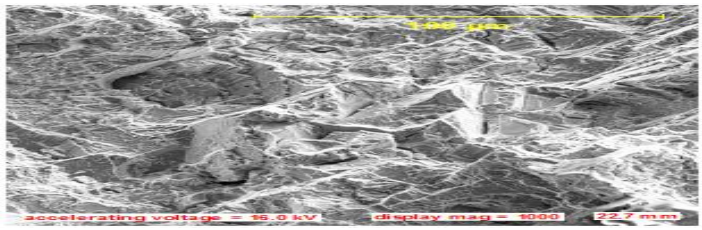
a) Rupture of the INC 718 blade at 1230K at 150MPa 4 ½ hrs



b) Rupture of the INC 718 blade at 1230K at 150MPa 4 ½ hrs



c) Rupture of the INC 718 blade at 1230K at 150 MPa 4 ½ hrs



d) Rupture of the INC 718 blade at 1242K at 150MPa 4 ½ h

Figure 4.19 (a-d): Microstructure of Ruptured INC 718 blade at 1230-1242K, at 150MPa.

4. **Conclusion**

I. In conclusion, the chemical composition analysis carried out on the three blade materials Ti, AISI 403 and Ni alloys after service life of 10,000 h each showed that their compositions (constituent elements) at room temperature was the same even after several heat treatment. The microstructures of the 1st, 2ndand 3rdstage of axial, single stage centrifugal compressors and single stage axial gas generator turbine at room temperature were different from the microstructures at 550K for Ti-alloys, 500K for AISI 403 cadmium stainless steel alloys and 1235K for Ni-alloys. These were the maximum temperature when fractures would occur in the presence of various loading conditions. For the dendritic structures of the three blades, during

heat treatment their γ, γ',$''$ microstructures were spherically shaped, their precipitates were thermodynamically stable, regular and evenly distributed in the γ matrix of the main element at room temperature. From the observations, it was concluded that γ', γ'' at room temperature were thermodynamically stable but would change their shapes at higher temperatures. HCL produced better etching than HNO_3 acid and it is also cheaper.

II. A load between 20-70 kN and tensile stress were applied between 150-175 MPa for low cycle fatigue during creep tests for all the blades from 1 -8 h. In the high cycle fatigue analysis, 962 MPa - 1245 MPa for Ni-alloy, 400 -750 MPa for Ti-alloy and 400- 650 MPa for stainless steel. The expected behavior in real life situation of the blades according to the manufacturer's specification, was that crack sizes per blade must not exceed 6 mm. It was concluded in this work having confirmed the presence of cracks to a maximum of 2 mm for stainless steel alloys, a low number of cycles of 10^6 should not be exceeded or rupture was imminent immediately. This was similar to precautions to be taken when a crack size of Ti, Ni-alloys blades detected were at 3 and 6.5 mm respectively, the blades' integrity could not be reliable after 10^8number of cycles hence permanent fracture would be inevitable.

5. Recommendations

1. Service history of the blades in turbine showed that the alloy composition should be looked into considering the severity of the environment they are subjected to,so that more resistance can be offered to thermal and centrifugal stresses which often cause quick deterioration of the blades integrity.
2. In INC 718 blades the γ', γ''particular carbides are strongly determined by their mechanical

properties, it is recommended that the strength of these precipitates should be improved upon and should well be ground with their inhibitive grain boundary agents considering the extreme temperature they are always subjected to.This has been found to pose negative impact on the mechanical properties of the blades after a number of cycles and hours of operation (Reed, 2006; Xu et al., 2012 and Cueto-Rodriguez et al. 2018).

3. Grain sizes of the hardening precipitates should be improved on so as to prevent early degradation of Ti-alloy and Ni-alloy blades of the compressor-turbine sections of the engine during in-service. This degradation could further lead to induced complex nonlinear vibration, also higher plastic deformation and even break off if not detected early. This phenomenon is hereby recommended for further studies in both axial gas and power generator turbines of the turboshaft engine being studied.

REFERENCES

Aabid A., Jyothi, Zayan J.M. and Khan S.A. (2019).Experimental and numerical investigation on gas turbine blade with the application of thermal barrier coatings.

Aabid, A. and Khan, S.A. (2018), "Optimization of heat transfer on thermal barrier coated gas turbine blade related", Proceedings of IOP Conference Series: Materials Science and Engineering, 370, 1-9. https://doi.org/10.1088/1757-899X/370/1/012022.

Ali, N.; Teixeira, J.A.; Addali, A.; Saeed, M.; Al-Zubi, F.; Sedaghat, A.; Bahzad, H. Deposition of Stainless Steel.

Alistair john (2017), Alleviation of shock-wave effects on a highly loaded axial compressor through novel blade shaping, Proceedings of ASME Turbo Expo 2016: Turbomachinery Technical Conference and Exposition. doi:10.1115/1.4035833.

Alqallaf J., Ali N., Teixeira J.A. and Addali A. (2020).Solid Particle Erosion Behaviour and Protective Coatings for Gas Turbine Compressor Blades. School of Aerospace, Transport and Manufacturing (SATM), Cranfield University, Cranfield MK43 0AL, UK; j.a.amaral.teixeira@cranfield.ac.uk (J.A.T.); Correspondence: j.alqallaf@cranfield.ac.uk. Received: 2 July 2020; Accepted: 7 August 2020; Published: 13 August 2020.

Bohorquez de Silva, Monica, "Study of microstructure effect on the thermal properties of Yttria-stabilized-Zirconia thermal barrier coatings made by atmospheric plasma spray and pressing machine" (2010). *LSU Doctoral Dissertations*. 855.https://digitalcommons.lsu.edu/gradschool_dissertations/855

Broek D (1985). A similitude criterion for fatigue crack growth modelling. Fracture Mechanics: 16th Symposium, 1985.

Broek, D. (1995). The Practical Use of Fracture Mechanics, Kluwer Academic Publisher, ISBN

Carney L.R, and Mecholsky J. J. (2013) Relationship between fracture toughness and fracture surface fractal dimension in AISI 4340 steel." (2013).

Carney L.R, and Mecholsky J. J. (2018). Characterization technique for

secondary and tertiary γ′ precipitates in Ni-based superalloys. Materials Characterization. 2018 Jun 1;140:86-94.

Chen Jun (2016).Status Quo and Development Trend of Advanced Aircraft Engine Resin Matrix Composites Technology. Aeronautical Manufacturing Technology, 2016, 500(5):68-72. 74

Chen, W.; Sun, Y.; Huo, D.; Teng, X. Modelling of the Influence of Tool Runout on Surface Generation in Micro Milling. Chin. J. Mech. Eng. 2019, 32, 2.

Chizhi Z; Hua-Peng C; Kong F.T. and Dongfang L. (2021).Reliability-Based Lifetime Fatigue Damage Assessment of Offshore Composite Wind Turbine Blades.

Comeli F.W, Rocha A.S, Silva de Oliveira C.A, Lemos G, and Castro R.M (2015).Effects of Tempering Temperature on the Microstructure and Creep Resistance of X22CrMoV12-1 Steel Used on Steam Turbine Blades.

Cordes T., Norton E., Brown H., Munson K (2019). Comparison of total fatigue life predictions of welded and machined A36 steel T-joints. SAE Technical Paper 2019-01-0527, 2019, https://doi.org/10.4271/2019-01-0527.

Dautov, S.S., Shornikov, P.G., Rezyapova, L.R. and Akhatov, I.S. (2019), “Increasing thermal and mechanical properties of thermal barrier coatings by suspension plasma spraying technology”, J. Phys.: Conference Series, 1281, 1-4. https://doi.org/10.1088/1742-6596/1281/1/012008

Deng D (2018) "Additively Manufactured Inconel 718 : MIcrostructures and Mechanical properties," Division of Engineering Materials Department of Management and Engineering Linköping University SE-581 83 Linköping, Sweden, Linköping , 2018

Di-Marco, P.C. Navy (2020) Foreign Object Damage and Its Impact on Future Gas Turbine Engine Low Pressure Compression Systems. In Agard Conference Proceedings AgardCp; AGARD: Rotterdam, The Netherlands, 1994; p. 6. Processes 2020, 8, 984 36 of 42.

Durand-Charre M. (2017).The microstructure of superalloys. Routledge; 2017 Nov 22.

Eddy Vanswijgenhoven and John Holmes (2016) Fatigue Crack Growth in Inconel 718 Superalloy Foil at Elevated Temperature.

Ekberg, Anders (2019). "Fatigue Crack Propagation" (PDF). Retrieved 6 July 2019

Farokhi, S. (2016), “Noise in a Nutshell,” AE 524, University of Kansas, Lawrence, KS 66045, 2016: 1-16.

Farokhi, S., Private Communication, February 2017.

Fei Xu (2020). Aircraft compressor application. Chin. J. Aeronaut. 2020, 33, 1824–1835.

for Scientific Research, Safat 13109, Kuwait; nmali@kisr.edu.kw

Francisco Miguel da Costa Baptista (2017).A 0-D Off-Design Performance Prediction Model of the CFM56-5B Turbofan Engine.

Frazier, W.E. (2014) "Metal Additive Manufacturing: A Review," Journal of Materials Engineering and Performance, vol. 23, no. 6, pp. 1917-1928, 2014.

Gao Yu, Li Yangyang, Wang Baichen (2016). Application of advanced resin matrix composites in aeroengine and its research progress. Manufacturing Technology, 2016(21): 16-21.

Garret.(2017). Compressor Maps. Retrieved from Honeywell Garret:

Giannella V., Perrella M., Shlyannikov V. N. (2018). Fatigue crack growth in a compressor stage of a turbofan engine by FEM-DBEM approach. Procedia Structural Integrity, Vol. 12, 2018, p. 404-415.

Goldberg, C.; Nalianda, D.; Sethi, V.; Pilidis, P.; Singh, R.; Kyprianidis, K (2018).Assessment of an energy-efficient aircraft concept from a techno-economic perspective. Appl. Energy 2018, 221, 229–238.

HamidrezaMoradi, Rafiullah Rafi, Abdullah Muslim (2021) Crack Growth Simulation In 13th Row Of Compressor Blades Under Foreign Object Damage And Resonant Vibration Condition.

Hanus M and Ruzicka (2016). Modeling of Damage of Turbine Blade

Haynes. International. HAYNES® 282® alloy, 2018

Iakimkin, V.; Kirillov, S.; Kirillov, A.; Pecht, M. (2018) Basic Principles, Models and Algorithms for Creation of Self-Maintenance and Self-Recovery Systems for Engines, Gas Turbines and Mechanics. In

Proceedings of the 2018 Prognostics and System Health Management Conference (PHM-Chongqing), Chongqing, China, 26–28 October 2018; pp. 270–275.

Ignacio Escobar-Moreno, M. V. Aguirre, Eva-María Andrés-López, Manuel José Viscasillas,

Daniel Barba (2019). Microstructural study of nickel-based superalloys through open source software of image analysis.ignacio.escobar.moreno@alumnos.upm.es.

Li L, Li C, Tang Y et al (2017) An integrated approach of reverse engineering aided remanufacturing process for worn components. Robot ComputIntegrManuf 48:39–50.

Lu, Y.-A.; Wang, C.-Y.; Zhou, L.; Sui, J.-B.; Zheng, L.-J. Smooth flank milling tool path generation for blade surfaces considering geometric constraints. Int. J. Adv. Manuf. Technol. 2019, 103, 1911–1923.

Perrut M., Caron P., Thomas M. and Couret A. (2018). High temperature materials for aerospace applications : Ni-based superalloys and γ-TiAl alloys. ComptesRendus Physique, Centre Mersenne, 2018, 19 (8), pp.657-671. 10.1016/j.crhy.2018.10.002. hal-02073852

Rayatpour, I., Z. Lalegani, Z. (2020) An Investigation of the Microstructural Evolution of a Service-Exposed Turbine Blade. Received: 2 July 2020; Accepted: 7 August 2020; Published: 13 August 2020

Rongqiao Wang, Kanghe Jiang, Fulei Jing, Dianyin Hu. Thermomechanical fatigue failure investigation on a single crystal nickel superalloy turbine blade. Engineering Failure Analysis, Elsevier, 2016,

10.1016/j.engfailanal.2016.04.016.hal-01324007

Sabila Kader Pinky (2020) Molecular Dynamics Study of Creep Deformation in Nickel-based Superalloy Missouri State University, SabilaKader760@live.missouristate.edu 2019

Singh, J.; Kumar, S.; Mohapatra, S.K. (2017).Tribological analysis of WC–10Co–4Cr and Ni–20Cr2O3 coating on stainless steel 304. Wear 2017, 376, 1105–1111.

Smith TM, Bonacuse P, Sosa J, Kulis M, Evans L (2018). A quantifiable and automated volume fraction.

Srinivas G, Raghunandana K and Satish Shenoy B (2018): Recent developments in turbomachinery component materials and manufacturing challenges for aero engine applications.

Steere, R.E.; Koepnick, E.G.; Dean, R.A. (2017). Progress on The Us Air Force Approach For The Practical Management Of Engine Life Cycle Costs. AGARD Lect. Ser. **2017**, 4, 1–4.

Su, C., Jiang, X., Huo, G. et al. Accurate model construction of deformed aero-engine blades for remanufacturing. Int J AdvManufTechnol 106, 3239–3251 (2020).https://doi.org/10.1007/s00170-019-04688-w

Vattappara K (2019) Production of Aircraft Engine Compressor Rotor Discs with Desired Service Life in Titanium Alloys. Vol. 10, Issue 3, Jun 2020, 13285–13296 © TJPRC Pvt. Ltd.

Yu J., Zhang S., Zhang Q., Liu R., Tang M., and Li X., (2016) “Simulation study and experiment verification of the creep mechanism of a nickel-based single crystal superalloy obtained from microstructural evolution,” RSC Adv.,

vol. 6, no. 109, pp. 107748–107758, 2016.

Zhang X, Li W, Liou F (2018) Damage detection and reconstruction algorithm in repairing compressor blade by direct metal deposition. Int J Adv ManufTechnol 95(5-8):2393–2404.

Funding & Support

This work was accomplished by the scholarship obtained from the Petroleum Technology Development Fund (PTDF) Abuja, Nigeria. The support received from the Nigerian Police Air Wing, Abuja and Material Laboratory Department, Kwara State University, Malete is acknowledged.